Proceedings of the XII International Symposium on Dynamic Problems of Mechanics (DINAME 2007),
P.S.Varoto and M.A.Trindade (editors), ABCM, Ilhabela, SP, Brazil, February 26 - March 2, 2007

On the Numerical Identification of the Bending Stiffness and the Damping of Transmission Line Conductors

Carlos Frederico Matt[1], **Daniel Alves Castello**[2]

[1] Electric Power Research Center (CEPEL), Avenida Um sem número, Ilha do Fundão, Cidade Universitária, Rio de Janeiro, Brazil, 21944-970, cfmatt@cepel.br

[2] Department of Mechanical Engineering, Universidade Federal Fluminense, Rua Passo da Pátria, 156, Niterói, Rio de Janeiro, Brazil, 24210-240, castello@mec.uff.br

Abstract: The most common type of conductors of high voltage transmission lines is composed of steel core wires and one to three layers of aluminum wires wound around, commonly referred to as ACSR conductors (Aluminum Conductor Steel Reinforced). Due to the complex geometry of a typical ACSR conductor under bending, the majority of the theoretical models available in the literature considers such a mechanical structure as a continuous system. In the simplest models the conductors are treated as taut strings without bending stiffness, while in the more sophisticated ones they are treated as homogeneous elastic beams with constant bending stiffness, and subjected to a constant axial load. Although the elastic beam model seems to be the most appropriate to describe the mechanical vibrations of transmission line conductors, such as the vibrations induced by the wind and commonly referred to as aeolian vibrations, there is a great uncertainty concerning the bending stiffness and the damping parameters of typical transmission line conductors. The present work is aimed at modelling transmission line conductors as homogeneous beams with viscous damping and estimating its bending stiffness and damping parameters. The mathematical formulation of the physical problem is developed under the framework of an Euler-Bernoulli beam subjected to small displacements. The direct problem is solved analytically and numerically by the generalized integral transform technique and the finite-element method, respectively. A suitable frequency-domain error function is defined as the sum of squares of the differences between measured and estimated frequency response functions. The inverse problem is aimed at minimizing this error function by means of the classical Levenberg-Marquardt parameter estimation technique. Several simulation examples have been performed in order to assess the effectiveness of the estimation procedures. Aiming at obtaining conditions closer to reality, the simulations are performed considering noise-corrupted measurements and a reduced number of available sensors over the structure.

Keywords: transmission line conductors, bending stiffness, damping, parameter estimation, Levenberg-Marquardt

INTRODUCTION

Wind-excited mechanical vibrations (or aeolian vibrations) in single overhead transmission line conductors are understood as a critical problem for the safety and reliability of the transmission line. Different types of mechanical vibrations may occur; however, the most common type corresponds to wind-excited vibrations in the frequency range of 3 Hz to 150 Hz, caused by vortex-shedding (Rawlins, 1979; Hagedorn, 1982; Meynen *et al.*, 2005). In the current work, the well-known galloping vibrations (CIGRÉ, 1989) of very low frequency (below 1 Hz) will not be considered. The aerodynamic lift force arising from the periodic shedding of vortices in the wake of the conductor is responsible for its subsequent vibrations in a direction normal to the wind flow. Depending on the pattern of the wind flow and on the mechanical damping of the transmission line, the dynamic stresses and strains induced on the constituent wires of the conductors may become dangerously high, especially at the suspension clamps and at the attachment points of Stockbridge dampers (Wagner *et al.*, 1973; Hagedorn, 1982; Hagedorn *et al.*, 1987). These stresses and strains may lead to fatigue damage on the wires with catastrophic consequences such as the complete rupture of the conductor and interruption on the supply of electric energy. Therefore, the understanding of the transmission lines dynamics is a relevant issue.

Aeolian vibrations on transmission line conductors are expected for wind speeds in the range of 1 m/s to 10 m/s. Based on typical values for conductor diameters (15 mm to 30 mm) and on the values of the dynamic viscosity and specific mass of the standard air, a simple calculation would reveal that such vibrations arise in wind flows with Reynolds number in the range of 10^3 to 10^4. For subsonic flows in this range of Reynolds number, also called sub-critical range, it is well-known that the shedding of vortices across stationary bluff bodies has a well-defined frequency, commonly referred to as the shedding frequency (Blevins, 1990). Experimental observations with stationary and smooth circular cylinders indicate that the shedding frequency, f_s, is directly proportional to the flow velocity normal to the cylinder, U, and inversely proportional to the cylinder diameter, D; the proportionality constant being the Strouhal number, St. It is also well-known that the Strouhal number is a function of both the geometry and Reynolds number for low Mach number flows (Blevins, 1990); for example, for smooth circular cylinders $\mathrm{St} \approx 0.2$ such that the stationary shedding frequency may be computed as $f_s = 0.2U/D$. Experimental measurements in the field have revealed that the Strouhal number for transmission line conductors are lies in the range 0.185 to 0.22 (Kraus and Hagedorn, 1991; Rao, 1995). The complicated phenomenon of

vortex-shedding across stationary bluff bodies is not yet completely understood and requires intense research efforts.

In the context of aeolian vibrations on overhead conductors, other complicating factors come into picture: (i) the dynamic interaction between the wind flow and the structural vibrations of the conductor; (ii) the irregular and apparently chaotic behavior of the wind flow; and (iii) the flexibility and surface roughness of transmission line conductors. Thereby, the subject of aeolian vibrations on transmission line conductors remains up to now unsatisfactorily explained, mainly because little progress has been made on the mathematical modelling of wind excitations and on the energy dissipated by stranded cables (as transmission line conductors) under flexural vibrations, which, in part, can be attributed to little data about the mechanical properties of transmission line conductors, such as the bending stiffness and damping parameters.

The most common type of conductors of high voltage transmission lines is composed of steel core wires and one to three layers of aluminum wires wound around, commonly referred to as ACSR conductors (Aluminum Conductor Steel Reinforced), as can be seen in Fig. 1. Under operational conditions, these conductors are subjected to a specified tensile mechanical load and their ends are clamped at the suspension towers. Due to the complex geometry of a typical ACSR

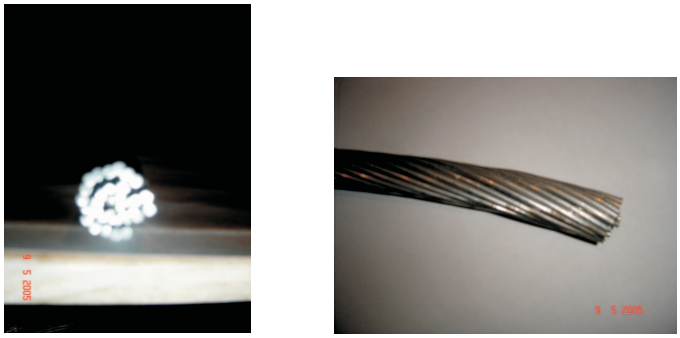

Figure 1 – ACSR transmission line conductor with three layers of aluminum wires.

conductor under bending, the majority of the theoretical models available in the literature considers such a mechanical structure as a continuous system (Claren and Diana, 1969; Dhotarad et al., 1978; Hagedorn, 1982; Hagedorn et al., 1987; Vecchiarelli et al., 2000; Diana et al., 2000; Matt and Castello, 2005). In the simplest models the conductors are treated as taut strings without bending stiffness, while in the more sophisticated ones they are treated as homogeneous elastic beams with constant bending stiffness, and subjected to a constant axial load. Although the elastic beam model seems to be more appropriate to describe the mechanical vibrations of transmission line conductors, there is a great uncertainty concerning the bending stiffness and the damping parameters of typical transmission line conductors.

The main mechanisms of damping on a transmission line conductor are now quite clear. Mechanical energy is dissipated due to the inter-strand friction among the constituent wires of the conductor (structural damping) and due to the aerodynamic losses during flexural vibrations (aerodynamic damping). In the literature, aerodynamic and structural damping are assumed to be, respectively, of viscous and hysteretic type; but few works have attempted to take these forms of damping into account. Energy is also dissipated due to material damping and at the conductor clamps. The measurement of the latter on a laboratory span seems to be a not very easy task.

As for the bending stiffness, Papailiou (1997) presented a more sophisticated model that takes into account the helicoidal geometry of the wires, the interlayer friction and the interlayer slip during bending. The model proposed by Papailiou (1997) leads to a variable bending stiffness, i.e., a stiffness which changes with the bending amplitude and the tension applied to the conductor. Matt and Castello (2005) also considered the transmission line conductor as a heterogeneous beam with a variable bending stiffness and estimated such a distributed property by the classical Levenberg-Marquardt iterative procedure. Nevertheless, most authors adopt a constant bending stiffness for the conductors. The constant value of the bending stiffness is frequently chosen to be within a certain range. The minimum value is obtained by considering the conductor as a bundle of individual wires and by assuming that all wires are free from each other to move; thus the minimum value is given by the sum of the bending stiffness of all wires (CIGRÉ, 1989). On the other hand, the maximum value is obtained by also considering the conductor as a bundle of individual wires and assuming that contact pressure among the wires is high enough to prevent their relative motions (CIGRÉ, 1989). The uncertainty about the bending stiffness of typical conductors is due to the fact that the maximum and minimum bending stiffness values may differ by several orders of magnitude.

The current work presents a model of transmission line conductors as homogeneous beams, taking into account aerodynamic and structural damping and estimating its bending stiffness and damping parameters. The mathematical formulation of the physical problem is developed under the framework of an Euler-Bernoulli beam subjected to small displacements. The direct problem is solved analytically and numerically by the generalized integral transform technique and the finite-element method, respectively. A suitable frequency-domain error function is defined as the sum of squares of the

differences between measured and estimated frequency response functions. The inverse problem is aimed at minimizing such an error function by means of the classical Levenberg-Marquardt parameter estimation technique.

This paper is organized as follows. In section 3, there is a description of the mathematical formulation of the physical problem under the framework of classical Euler-Bernoulli beam subjected to axial tensile load and small displacements, a formulation the direct problem, and a discussion of its analytical and numerical solutions. Then, the classical Levenberg-Marquardt iterative procedure is presented. In section 4, the estimates obtained for the bending stiffness and damping parameters are presented and analyzed. Finally, in section 5, the main conclusions and comments about future works are stated.

MATHEMATICAL FORMULATION OF THE PHYSICAL PROBLEM

In the the present work the transmission line conductor is modelled as an Euler-Bernoulli beam with constant bending stiffness EI and subjected to a constant tensile load T. Figure 2 shows a differential element of a transmission line

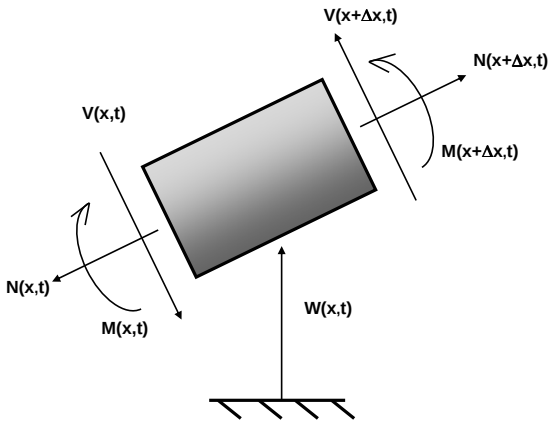

Figure 2 – Differential element of the transmission line conductor.

conductor. Based on Figure 2, one can write the balance of forces along the vertical direction as

$$H(x,t)\,\Delta x + \left[T + \frac{\partial T}{\partial x}\Delta x\right]\left[\frac{\partial w}{\partial x} + \frac{\partial^2 w}{\partial x}\Delta x\right] + \left[V + \frac{\partial V}{\partial x}\Delta x\right] - T\frac{\partial w}{\partial x} - V - \alpha\frac{\partial w}{\partial t}\Delta x = \rho A\Delta x\frac{\partial^2 w}{\partial t^2}, \tag{1}$$

which leads to

$$H(x,t) + \frac{\partial}{\partial x}\left(T\frac{\partial w}{\partial x}\right) + \frac{\partial T}{\partial x}\frac{\partial^2 w}{\partial x^2}\Delta x + \frac{\partial V}{\partial x} - \alpha\frac{\partial w}{\partial t} = \rho A\frac{\partial^2 w}{\partial t^2}. \tag{2}$$

where $H(x,t)$ stands for the external excitation, ρ denotes the specific mass of the conductor and A its cross-section area. The product ρA represents the mass per unit length of the conductor and will henceforth be denoted by the symbol μ. The fifth term on the left side of Eq. (2) stands for an aerodynamic damping of viscous type. The parameter α appearing on Eq. (2) is the equivalent viscous damping constant. If one disregards rotational inertia, the bending moment $M(x,t)$ is related to the shear force $V(x,t)$ as follows

$$\frac{\partial M}{\partial x} + V = 0, \tag{3}$$

which leads to

$$H(x,t) + \frac{\partial}{\partial x}\left(T\frac{\partial w}{\partial x}\right) + \frac{\partial T}{\partial x}\frac{\partial^2 w}{\partial x^2}\Delta x - \frac{\partial^2 M}{\partial x^2} - \alpha\frac{\partial w}{\partial t} = \mu\frac{\partial^2 w}{\partial t^2}. \tag{4}$$

Taking the limit as Δx goes to zero, one arrives at

$$H(x,t) + \frac{\partial}{\partial x}\left(T\frac{\partial w}{\partial x}\right) - \frac{\partial^2 M}{\partial x^2} - \alpha\frac{\partial w}{\partial t} = \mu\frac{\partial^2 w}{\partial t^2}. \tag{5}$$

In order to obtain the final form of the equation of motion, it is necessary to express the bending moment $M(x,t)$ as a function of the displacement field $w(x,t)$, what can be done after choosing a suitable constitutive equation for the medium. As a first approach, one may consider the following constitutive equation

$$\sigma = E\varepsilon + \xi\frac{\partial \varepsilon}{\partial t}. \tag{6}$$

where E and ξ are, respectively, the Young modulus and the material damping factor. In this initial approach, one should assume that the second term on the right side of Eq. (6) takes into account all the losses but the aerodynamic one. It should be highlighted that although this damping model is quite simple, Barbieri et al. (2004) used a similar model to characterize the dynamic behavior of a transmission line conductor and their simulated results got closer to the experimental ones.

Using Eq. (6), the bending moment $M(x,t)$ may be written as follows

$$M(x,t) = \int_A -y\,\sigma(x,t)\,dA = \int_A -y\left[E\varepsilon + \xi\,\frac{\partial \varepsilon}{\partial t}\right] dA \tag{7}$$

where the strain field, for small displacements of the conductor, may cast as follows

$$\varepsilon(x,y,t) = \frac{T}{EA} - y\frac{\partial^2 w}{\partial x^2}. \tag{8}$$

The bending moment $M(x,t)$ is finally given as follows

$$M(x,t) = EI\frac{\partial^2 w}{\partial x^2} + \xi I\frac{\partial^3 w}{\partial x^2 \partial t} \tag{9}$$

and the following relations have been used

$$\int_A y\,dA = 0 \;\text{ and }\; I \equiv \int_A y^2\,dA. \tag{10}$$

Substituting Eq. (9) into Eq. (5) one arrives at the following equation

$$H(x,t) + \frac{\partial}{\partial x}\left(T\frac{\partial w}{\partial x}\right) - \frac{\partial^2}{\partial x^2}\left[EI\frac{\partial^2 w}{\partial x^2}\right] - \frac{\partial^2}{\partial x^2}\left[\xi I\frac{\partial^3 w}{\partial x^2 \partial t}\right] - \alpha\frac{\partial w}{\partial t} = \mu\,\frac{\partial^2 w}{\partial t^2}. \tag{11}$$

Considering the tensile load T, the bending stiffness EI and the internal dissipation ξI as constants, the final form of the equation of motion may be written in the following form

$$EI\,\frac{\partial^4 w}{\partial x^4} - T\,\frac{\partial^2 w}{\partial x^2} + \xi I\,\frac{\partial}{\partial t}\left(\frac{\partial^4 w}{\partial x^4}\right) + \alpha\frac{\partial w}{\partial t} + \mu\,\frac{\partial^2 w}{\partial t^2} = H(x,t). \tag{12}$$

Direct Problem

The direct problem consists in finding the solution of Eq. (12), satisfying the appropriate boundary and initial conditions, with the conductor parameters EI, ξI and α, and the excitation $H(x,t)$ known *a priori*. Several analytical techniques and numerical methods may be used to solve the direct problem. Here, the direct problem is solved through the finite-element method (Hughes, 2000; Reddy, 1993) and the generalized integral transform technique (Özişik, 1993; Cotta, 1993).

Numerical solution by the finite-element method

The numerical solution of Eq. (12) will be obtained by means of the Finite Element Method. Multiplying the equation of motion by a test function u and integrating it over a sub-domain of the system leads to

$$\int_{x_e}^{x_{e+1}} \left(-T\frac{\partial w}{\partial x}\frac{\partial u}{\partial x} - EI\frac{\partial^2 w}{\partial x^2}\frac{\partial^2 u}{\partial x^2} - \xi I\frac{\partial^3 w}{\partial x^2 \partial t}\frac{\partial^2 u}{\partial x^2} - \alpha\frac{\partial w}{\partial t}u - \mu\frac{\partial^2 w}{\partial t^2}u + Hu\right) dx = 0 \tag{13}$$

Considering that the displacement field can be approximated by $w(x,t) = \mathbf{N}(x)\mathbf{w}_h(t)$ one obtains

$$\int_{x_e}^{x_{e+1}} \left(-T\frac{\partial \mathbf{N}}{\partial x}^T\frac{\partial \mathbf{N}}{\partial x}\mathbf{w}_h\cdot\mathbf{u}_h - EI\frac{\partial^2 \mathbf{N}}{\partial x^2}^T\frac{\partial^2 \mathbf{N}}{\partial x^2}\mathbf{w}_h\cdot\mathbf{u}_h + \right. \tag{14}$$

$$\left. +(-1)\xi I\frac{\partial^2 \mathbf{N}}{\partial x^2}^T\frac{\partial^2 \mathbf{N}}{\partial x^2}\dot{\mathbf{w}}_h\cdot\mathbf{u}_h - \alpha\mathbf{N}^T\mathbf{N}\dot{\mathbf{w}}_h\cdot\mathbf{u}_h - \mu\mathbf{N}^T\mathbf{N}\ddot{\mathbf{w}}_h\cdot\mathbf{u}_h + H\,\mathbf{N}^T\mathbf{u}_h\right) dx + \Gamma = 0$$

where $\mathbf{N}$ is a matrix containing the shape functions and Γ contains the boundary conditions. In matrix form, the evolution equation casts as

$$\mathbf{M}^e\ddot{\mathbf{w}}_h + \mathbf{D}^e\dot{\mathbf{w}}_h + \mathbf{K}^e\mathbf{w}_h = \mathbf{f}^e \tag{15}$$

where

$$\mathbf{M}^e = \int_{x_e}^{x_{e+1}} \mu\, \mathbf{N}^T \mathbf{N}\, dx \tag{16}$$

$$\mathbf{K}^e = \int_{x_e}^{x_{e+1}} \left(EI \frac{\partial^2 \mathbf{N}}{\partial x^2}^T \frac{\partial^2 \mathbf{N}}{\partial x^2} + T \frac{\partial \mathbf{N}}{\partial x}^T \frac{\partial \mathbf{N}}{\partial x} \right) dx \tag{17}$$

$$\mathbf{D}^e = \int_{x_e}^{x_{e+1}} \left(\xi I \frac{\partial^2 \mathbf{N}}{\partial x^2}^T \frac{\partial^2 \mathbf{N}}{\partial x^2} + \alpha \mathbf{N}^T \mathbf{N} \right) dx \tag{18}$$

The elemental damping matrix can be rewritten as a function of the elemental mass and stiffness matrices as follows:

$$\mathbf{D}^e = \frac{\alpha}{\mu}\mathbf{M}^e + \int_{x_e}^{x_{e+1}} \xi I \frac{\partial^2 \mathbf{N}}{\partial x^2}^T \frac{\partial^2 \mathbf{N}}{\partial x^2}\, dx = \frac{\alpha}{\mu}\mathbf{M}^e + \frac{\xi}{E}\mathbf{K}^e - \frac{\xi T}{E} \int_{x_e}^{x_{e+1}} \frac{\partial \mathbf{N}}{\partial x}^T \frac{\partial \mathbf{N}}{\partial x}\, dx. \tag{19}$$

Analytical solution by the generalized integral transform technique

The first task in applying the generalized integral transform technique to solve Eq. (12) is to define the inverse-transform pair. Based on the solution of the equation of motion for the undamped free vibrations of the conductor (Eq. (12) with $H(x,t) = 0$ and $\alpha = \xi = 0$), the inverse-transform pair is defined as

$$\bar{w}_m(t) = \int_0^L \Psi_m(\lambda_m, x)\, w(x,t)\, dx \quad \text{(transform)} \tag{20}$$

$$w(x,t) = \sum_{m=1}^{\infty} \frac{\Psi_m(\lambda_m, x)}{N(\lambda_m)}\, \bar{w}_m(t) \quad \text{(inverse)}, \tag{21}$$

where λ_m and $\Psi_m(\lambda_m, x)$ denote, respectively, an undamped natural frequency and the mode of vibration (eigenvalue and corresponding eigenfunction), and $N(\lambda_m)$ stands for the norm of the eigenfunction $\Psi_m(\lambda_m, x)$. The eigenvalues λ_m and corresponding eigenfunctions $\Psi_m(\lambda_m, x)$, $m = 1, 2, \ldots, \infty$, depend upon the boundary conditions. In what follows, one may assume a concentrated harmonic excitation of the kind $H(x,t) = H_0\, \mathrm{e}^{i\Omega t}\, \delta(x - x_s)$, where H_0, Ω and $x_s \in\,]0, L[$ are, respectively, the amplitude, circular frequency and position of the excitation.

Multiplying Eq. (12) by $\Psi_m(\lambda_m, x)$, integrating in x from 0 to L, using the definition of $\bar{w}_m(t)$, evaluating the resulting integrals by parts and using the appropriate boundary conditions for $w(x,t)$ and $\Psi_m(\lambda_m, x)$, one derives the following system of coupled second-order ordinary differential equations for the transformed displacements $\bar{w}_m(t)$:

$$\frac{d^2 \bar{w}_m}{dt^2} + 2\zeta_m^* \lambda_m \frac{d \bar{w}_m}{dt} + \frac{\xi I}{EI} \frac{T}{\mu} \sum_{n=1}^{\infty} \Lambda_{mn} \frac{d \bar{w}_n}{dt} + \lambda_m^2\, \bar{w}_m = \frac{H_0}{\mu}\, \Psi_m(\lambda_m, x_s)\, \mathrm{e}^{i\Omega t}, \tag{22}$$

where $\zeta_m \equiv \frac{\alpha}{2\mu\lambda_m}$, $\zeta_m^* \equiv \zeta_m + \frac{1}{2}\frac{\xi I}{EI}\lambda_m$ and the coupling matrix Λ_{mn}, $m, n = 1, 2, \ldots, \infty$, is defined by

$$\Lambda_{mn} \equiv \frac{1}{N(\lambda_n)} \int_0^L \Psi_n(\lambda_n, x) \frac{d^2 \Psi_m}{dx^2}\, dx = -\frac{1}{N(\lambda_n)} \int_0^L \frac{d\Psi_n}{dx} \frac{d\Psi_m}{dx}\, dx. \tag{23}$$

The last expression appearing on Eq. (23) may be easily derived by performing integration by parts and using the appropriate boundary conditions for $\Psi_m(\lambda_m, x)$ and $\Psi_n(\lambda_n, x)$. It should be noted that the coupled system of ordinary-differential equations in Eq. (22) becomes uncoupled if and only if $\xi = 0$ or $T = 0$ or Λ_{mn} is a diagonal matrix. This coupled system of ordinary differential equations may be solved numerically after truncating the infinite series into a finite number of terms, say N_T. Once the transformed displacements $\bar{w}_m(t)$, $m = 1, 2, \ldots, N_T$, are obtained, the original displacement field $w(x,t)$ is easily recovered with the aid of Eq. (21).

Based on the linearity of the system (22), it is reasonable to assume a steady-state harmonic solution for $\bar{w}_m(t)$ of the kind $\bar{w}_m(t) = W_m\, \mathrm{e}^{i\Omega t}$. Substituting the harmonic solution for $\bar{w}_m(t)$ into Eq. (22), one arrives at the following system of algebraic equations for the complex amplitudes W_m

$$\sum_{n=1}^{N_T} K_{mn} W_m = F_m, m = 1, 2, \ldots, N_T. \tag{24}$$

The components of the coefficient matrix and forcing vector are given by the following expressions:

$$K_{mn} = \left(\lambda_n^2 - \Omega^2\right) \delta_{mn} + i \left(2\zeta_n^* \lambda_n \Omega\, \delta_{mn} + \frac{\xi I}{EI} \frac{T}{\mu} \Omega \Lambda_{mn} \right) \quad \text{and} \quad F_m = \frac{H_0}{\mu}\, \Psi_m(\lambda_m, x_s). \tag{25}$$

The symbol δ_{mn} denotes de Kronecker delta. Defining the complex frequency response function, $\hat{H}(x, x_s, \Omega)$ as the quotient of the amplitude of the acceleration (response) divided by the amplitude of the excitation, H_0, one has

$$\hat{H}(x, x_s, \Omega) = -\Omega^2 \sum_{m=1}^{N_T} \frac{\Psi_m(\lambda_m, x)}{N(\lambda_m)} \frac{W_m}{H_0}. \tag{26}$$

Inverse Problem

For the inverse problem of parameter estimation considered in this work, the conductor bending stiffness, EI, and the viscous damping coefficient, α, are regarded as unknown. The additional information used to estimate these two parameters are the complex frequency response functions measured at prescribed locations $x = x_p$, $p = 1,2,\ldots,N_s$, along the conductor and at circular frequencies Ω_q, $q = 1,2,\ldots,N_f$, where N_s is the number of sensors and N_f is the number of frequency data. The boundary value problem given by Eq. (12), with EI and α regarded as unknown, constitutes an inverse problem in which the parameters EI and α are to be estimated. The solution of this inverse problem for the estimation of the above two parameters is based on the minimization of the ordinary least squares norm given by (Özişik and Orlande, 2000)

$$S(\mathbf{P}) = \sum_{p=1}^{N_s} \sum_{q=1}^{N_f} \left(\hat{H}_{pq}^{\text{meas.}} - \hat{H}_{pq}^{\text{est.}}(\mathbf{P})\right)^* \left(\hat{H}_{pq}^{\text{meas.}} - \hat{H}_{pq}^{\text{est.}}(\mathbf{P})\right). \tag{27}$$

where $(\bullet)^*$ denotes the complex conjugate; $S(\mathbf{P})$ is the sum of square errors or objective function which is to be minimized; $\mathbf{P}^T$ is the two-column vector of unknown parameters (here, $P_1 = EI$ and $P_2 = \alpha$); $\hat{H}_{pq}^{\text{meas.}}$ and $\hat{H}_{pq}^{\text{est.}}(\mathbf{P})$ are, respectively, the measured and estimated complex frequency response functions, both evaluated at locations $x = x_p$, $p = 1,2,\ldots,N_s$ and at frequencies Ω_q, $q = 1,2,\ldots,N_f$. The minimization of $S(\mathbf{P})$, given by Eq. (27), is carried out by means of the classical Levenberg-Marquardt iterative procedure for parameter estimation (Levenberg, 1944; Marquardt, 1963; Beck and Arnold, 1977; Özişik and Orlande, 2000; Matt and Castello, 2005). The computation of the sensitivity matrix is required for the estimation process. In fact, for its computation, it is necessary to obtain the derivatives of the estimated frequency response functions with respect to EI and α. In the present work, finite-difference approaches were used in order to compute the derivatives of the estimated frequency response functions with respect to the unknown parameters EI and α (Özişik and Orlande, 2000; Matt and Castello, 2005).

RESULTS AND CONCLUSIONS

Aiming at assessing the effectiveness of the proposed methodology to estimate the bending stiffness and damping parameters, some simulation results are presented and analyzed in this section. The values chosen in the simulations for the dimensions and mechanical properties are typical of transmission line conductors tested on the laboratory span of Electric Power Research Center (CEPEL). Hence, in our simulation results, the axial mechanical load T, the span length L, the mass per unit length μ, the bending stiffness EI, the viscous damping coefficient α and the internal damping factor ξ were chosen to be equal to $10700\,\text{N}$, $65.355\,\text{m}$, $0.8127\,\text{kg/m}$, $11.07\,\text{N}\cdot\text{m}^2$, $0.08127\,\text{N}\cdot\text{s/m}^2$ and $1.1\times10^{-4}\,\text{N}\cdot\text{s/m}^2$, respectively. Three accelerometers have been considered in order to provide the pseudo-experimental frequency response functions (FRFs). They are located at the positions $L/4$ (AC1), $L/2$ (AC2) and $3L/5$ (AC3). The driving point for the FRFs is located at the same position of the accelerometer AC3. Accelerometers AC1 and AC2 are used for the estimation process.

In order to realistically simulate the corrupting effects of noise, filtering, digital sampling and truncation of the modal spectrum, a virtual simulator was utilized. The simulator estimates the FRF for each input-output pair through ensemble averaging. In order to achieve a higher level of fidelity, the input signal is pre-filtered before the analog conversion. The noise contaminated system response is the available one to be processed, and this signal is filtered at 80% of the Nyquist frequency before digital sampling. As reported in Alvin (1995), this procedure furnishes realism to the FRF obtaining problem. The pseudo-experimental FRFs were obtained with a finite-element model of the Euler-Bernoulli beam containing one hundred elements whose time domain responses were noise-corrupted. The noise level is measured by the standard signal-to-noise ratio (SNR) which is defined as follows:

$$\text{SNR} = 10\log\frac{\sigma_s^2}{\sigma_n^2} \tag{28}$$

where σ_s and σ_n denote, respectively, the standard-deviations of the signal and noise. The frequency band used for the estimations was chosen to be from 0 to 20 Hz. A large number of frequency data points (six hundred and eighty three) was used in order to have well-defined resonance and anti-resonance regions in the frequency response functions. It should be emphasized that, in the frequency range adopted, there are approximately twenty-three natural frequencies, closely spaced.

All the simulations considered simple-supported ends and the following initial guesses for the unknown parameters: $EI^{(0)} = 10^{-1}\,\text{N}\cdot\text{m}^2$ and $\alpha^{(0)} = 10^{-3}\,\text{N}\cdot\text{s/m}^2$. As previously presented, the true values of the above mentioned parameters are $EI = 11.07\,\text{N}\cdot\text{m}^2$ and $\alpha = 0.08127\,\text{N}\cdot\text{s/m}^2$. The first case studied considers the pseudo-experimental frequency response functions generated with $\text{SNR} = 90\,\text{dB}$ (low noise level). Table 1 shows the estimation results obtained through the models based on the generalized integral transform (GITT) and the finite element method (FEM), as a function of the number of series terms (N_T) and the number of elements (N), respectively. From Table 1 one can clearly see that the parameter α is effectively estimated. It should be emphasized that the solution obtained with the GITT model does not change with the number of series terms (N_T) indicated on Table 1. On the other hand, the solution obtained with the FEM

Table 1 – Estimated bending stiffness and aerodynamic damping coefficient with $\mathrm{SNR} = 90\,\mathrm{dB}$ **(case 1).**

GITT			FEM		
N_T	EI	α	N	EI	α
100	16.428	0.0817	40	13.626	0.0826
150	16.428	0.0817	60	16.721	0.0822
200	16.428	0.0817	80	17.065	0.0819

model gets closer to the true value as the number of elements (N) increases to eighty. Concerning the bending stiffness parameter, it is clear that the provided results are overestimated by 50%, approximately.

The second case to be analyzed considers everything equal to case one, except the signal-to-noise ratio, which is now considered to be 20 dB (high noise level). Table 2 shows the results obtained for the second case. From Table 2, one can draw the same conclusions stated for case one. Although the magnitude of the noise for the second case is much larger than the one for the first case, subtle variations on the estimated parameters were observed. The authors attribute these slight variations to the fact that the peaks in the pseudo-experimental frequency response functions remain well-defined, even for a high level of noise (see, for example, Fig. 3). From the analysis of Tables 1 and 2 it is easy to verify that

Table 2 – Estimated bending stiffness and aerodynamic damping coefficient with $\mathrm{SNR} = 20\,\mathrm{dB}$ **(case 2).**

GITT			FEM		
N_T	EI	α	N	EI	α
100	16.436	0.0817	40	13.627	0.0826
150	16.436	0.0817	60	16.650	0.0822
200	16.436	0.0817	80	17.065	0.0818

there is no agreement between the estimated and exact values for the bending stiffness. A simple sensitivity analysis around the estimated solution reveals that, in the frequency range adopted, the sensitivity of the response of the system to parameter α is much larger than its sensitivity to the bending stiffness. In fact, one can also conclude that the lower the frequency, the less sensitive the system becomes to the bending stiffness; therefore, the estimation process gets harder to be accomplished. Based on the numerical experiments performed in this work, the authors conclude that, in order to improve the estimates for the bending stiffness, higher frequencies (in the range of 50 Hz to 80 Hz) must be taken into account during the estimation process.

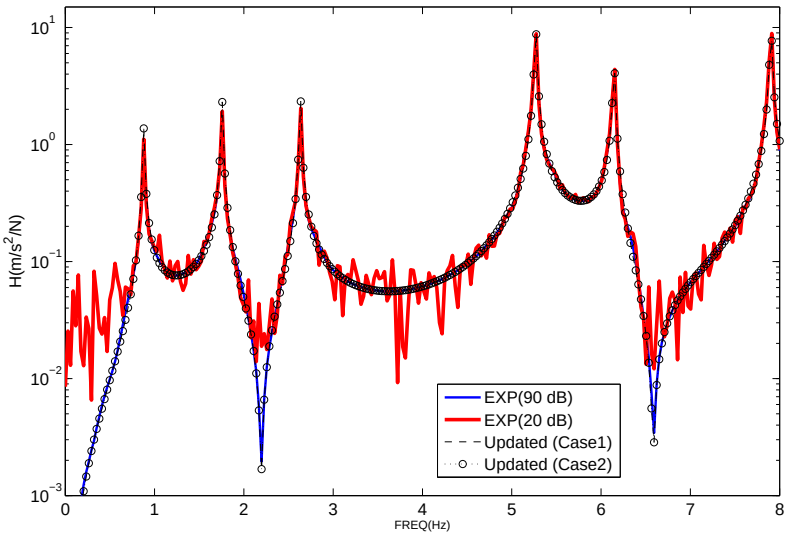

Figure 3 – Comparison of the pseudo-experimental and estimated frequency response functions for the frequency band (0, 8) Hz.

Experimental evidences on a laboratory span indicate that part of the energy provided by the excitation source is dissipated at the conductor clamps. Based on this information and in order to make the experimental simulated data closer to reality, for the third case the authors decided to include a concentrated dissipation at the ends of the FEM model used to generate the pseudo-experimental FRFs. These concentrated dissipations are modelled as viscous rotational dampers at $x = 0$ and at $x = L$ with damping constants equal to $c_0 = c_L = 10\,\mathrm{N{\cdot}m{\cdot}s/rad}$. Few works have attempted to quantify such concentrated dissipation in terms of the energy input by the excitation source; therefore, the values of c_0 and c_L adopted in the simulations may be unrealistic. The model which is going to be used for the estimation process does not take into account such concentrated dissipations. The objective here is to verify how concentrated dissipations not included in the theoretical model may affect the estimation process. Table 3 shows the results obtained for the third case with a high level

Table 3 – Estimated bending stiffness and aerodynamic damping coefficient with $\mathrm{SNR} = 20\,\mathrm{dB}$ **and concentrated dissipation at the conductor ends (case 3).**

GITT			FEM		
N_T	EI	α	N	EI	α
100	48.238	0.2566	40	44.795	0.2706
150	48.238	0.2565	60	47.992	0.2681
200	48.238	0.2565	80	48.382	0.2676

of noise (SNR = 20 dB). Because of the concentrated dissipations, both the bending stiffness and the viscous damping coefficient are largely overestimated. Similar results to the ones indicated on Table 3 were obtained for other levels of noise and damping constants c_0 and c_L. The important conclusion extracted from Table 3 is that if the concentrated dissipation at the ends are not negligible, the values obtained for the conductor bending stiffness and damping parameters may be quite far away from their exact values. Hence, knowing the order of magnitude of the energy dissipated at conductor clamps is highly desirable. Only in this way, the researchers will be able to judge if such concentrated dissipations shall be included or not in the theoretical models.

In order to reproduce real-like experimental shortcomings, the authors decided to analyze the effects of model uncertainties on the estimated parameters. In the fourth case, the authors assume an uncertainty of +5 cm in the model span length L, which corresponds to 0.08% of the span length. It should be emphasized that the pseudo-experimental FRFs are the same used for case 1, i.e., they were built based on the nominal parameters (defined in the first paragraph of section 4) and with no dissipation at the conductor ends. Table 4 shows the results obtained for case 4. For the sake of simplicity,

Table 4 – Estimated bending stiffness and aerodynamic damping coefficient with $\mathrm{SNR} = 90\,\mathrm{dB}$**, considering an uncertainty of +5 cm (+0.08%) in the span length** L**.**

GITT				FEM			
EI	$\Delta EI(\%)$	α	$\Delta\alpha(\%)$	EI	$\Delta EI(\%)$	α	$\Delta\alpha(\%)$
34.233	209	0.08715	7	31.163	182	0.08346	3

the authors decided to define an error measure associated to the estimated parameters. This error measure is defined as follows:

$$\Delta P = \frac{|\hat{P} - P^{\mathrm{exact}}|}{P^{\mathrm{exact}}} \times 100\% \tag{29}$$

where $\hat{P}$ and P^{exact} denote, respectively, the estimated and the exact parameter values. From the analysis of Table 4 three points should be remarked. First, the error for the estimated bending stiffness is much larger than the one for the estimated aerodynamic damping coefficient. While one is acceptable (7%-GITT, 3%-FEM) for the parameter α, the other one, for the bending stiffness EI, is around 200%. Second, the large discrepancies verified for the bending stiffness are associated with the low sensitivity of the objective function with respect to this parameter in the analyzed frequency band. For instance, considering the same estimation problem analyzed in case 4 but reducing the frequency band from (0, 20) Hz to (0, 10) Hz provides the results $EI = 105.35$ ($\Delta EI = 852\%$) and $\alpha = 0.0878$ ($\Delta\alpha = 8\%$), when the FEM model is used. Third, an increase in the estimated bending stiffness was already expected inasmuch as an increase in the span length reduces the stiffness of the system.

In the fifth case, the authors assume an uncertainty of -214 N in the model mechanical load T, which corresponds to -2% of the mechanical load. It should be emphasized that such percentage variation is expected in the laboratory tests with actual transmission line conductors. Table 5 shows the results obtained for case 5. From Table 5 one may note that the levels of error for both parameters are very high. Obviously, the increase in the bending stiffness is a straightforward

Table 5 – Estimated bending stiffness and aerodynamic damping coefficient with $\mathrm{SNR} = 90\,\mathrm{dB}$, considering an uncertainty of -214 N (-2%) in the mechanical load T.

GITT				FEM			
EI	$\Delta EI(\%)$	α	$\Delta\alpha(\%)$	EI	$\Delta EI(\%)$	α	$\Delta\alpha(\%)$
228.35	1963	0.3064	277	225.26	1940	0.444	446

result due to the fact that the decrease in the mechanical load leads to a decrease in the stiffness of the system. At the present moment no further conclusions can be stated for this last case which demands more numerical experiments.

CONCLUDING REMARKS AND COMMENTS FOR FUTURE WORKS

In the present work the transmission line conductors were modelled as homogeneous beams with viscous damping and their bending stiffness and damping parameters were estimated. The mathematical formulation of the physical problem was developed under the framework of an Euler-Bernoulli beam subjected to small displacements. The direct problem was solved analytically, by means of the GITT technique, and numerically, by means of the finite element method. A suitable frequency-domain error function was defined as the sum of squares of the differences between measured and estimated frequency response functions. The inverse problem comprised the minimization of such an error function by means of the classical Levenberg-Marquardt parameter estimation technique. Several simulation examples have been performed in order to assess the effectiveness of the estimation procedures. Aiming at obtaining conditions closer to reality, the simulations were performed considering a reduced number of available sensors over the structure and noise-corrupted measurements.

For the cases analyzed in this work, the main conclusions are: (i) the objective function is much less sensitive to the bending stiffness than the aerodynamic damping coefficient in the frequency band (0, 20) Hz; (ii) the estimates for the aerodynamic damping coefficient were, in general, in agreement with its exact value; (iii) the estimated parameters were practically unaffected by the considered levels of signal-to-noise ratio; (iv) the uncertainty in the span length affected much more the bending stiffness than the aerodynamic damping coefficient; (v) the uncertainty in the mechanical load largely affected both parameters.

The main contributions of the current work are: the numerical analysis of the estimation of two parameters of transmission line conductors, namely, the bending stiffness and the aerodynamic damping coefficient and the use of GITT technique to solve the associated direct problem. The numerical analyses have taken into account the effect of model uncertainties on the estimated parameters what, to the authors belief, are not considered in the literature for this specific problem. As for the direct problem, the authors would like to highlight that, although they also solved it by means of the FEM method, they did not have any intention of making comparisons; the main purpose was to have two ways to solve it. Lastly, for future works, the authors intend to extend the estimation procedure for higher frequency bands, to improve the damping models and to perform experimental analyses.

ACKNOWLEDGEMENTS

The authors would like to gratefully thank M.Sc. Bianca Walsh for all her kindly suggestions and hints.

REFERENCES

[1] Alvin, K. F., 1995, ”Method for Determining Minimum-order Mass and Stiffness Matrices from Modal Test Data”, AIAA Journal, Vol. 33, pp. 128-135.

[2] Barbieri, N., de Souza, O. H. and Barbieri, R., 2004, ”Dynamical analysis of transmission line cables. Part 1 - Linear Theory,” Mechanical Systems and Signal Processing, Vol. 18, pp. 659-669.

[3] Beck, J. V. and Arnold, K. J., 1977, ”Parameter estimation in engineering and science”, Wiley, New York, 501p.

[4] Blevins, R. D., ”Flow Induced Vibrations”, 2nd Edition, New York, Van Nostrand Reinhold, 1990, 477p.

[5] CIGRÉ SC 22 WG 01, 1989, ”Report on aeolian vibration”, Electra, Vol. 124, pp. 41-77.

[6] Claren, R. and Diana, G., 1969, ”Mathematical analysis of transmission line vibration”, IEEE Transactions on Power Apparatus and Systems, Vol. 88, No. 12, pp. 1741-1771.

[7] Cotta, R. M., 1993, ”Integral Transforms in Computational Heat and Fluid Flow”, CRC Press, Boca Raton, Florida, 352p.

[8] Dennis, J. and Schnabel, R., 1983, ”Numerical methods for unconstrained optimization and nonlinear equations”, Prentice Hall, Inc., 378p.

[9] Dhotarad, M. S., Ganesan, N. and Rao, B. V. A., 1978, ”Transmission line vibrations”, Journal of Sound and Vibration, Vol. 60, No. 2, pp. 217-237.

[10] Diana, G., Falco, M., Cigada, A. and Manenti, A., 2000, ”On the Measurement of Overhead Transmission Line Conductor Self-Damping”, IEEE Transactions on Power Delivery, Vol. 15, No. 1, pp. 285-292.

[11] Hagedorn, P., 1982, ”On the computation of damped wind-excited vibrations of overhead transmission lines”, Journal of Sound and Vibration, Vol. 83, No. 2, pp. 253-271.

[12] Hagedorn, P., Schmidt, J. and Nascimento, N., 1987, ”Stochastic field processes in the mathematical modelling of damped transmission line vibrations”, Mathematical Modelling, Vol. 8, pp. 359-363.

[13] Hughes, T. J. R., 2000, ”The finite element method - Linear static and dynamic finite element analysis”, Dover Publications, Inc., New York, 682p.

[14] Kraus, M. and Hagedorn, P., ”Aeolian Vibration: Wind Energy Input Evaluated from Measurements on an Energized Transmission Line”, 1991, IEEE Transactions on Power Delivery, Vol. 6, No. 3, pp. 1264-1270.

[15] Levenberg, K., 1944, ”A method for the solution of certain non-linear problems in least squares”, Quarterly Applied Mathematics, Vol. 2, pp. 164-168.

[16] Marquardt, D. W., 1963, ”An algorithm for least squares estimation of nonlinear parameters”, Journal of the Society for Industrial and Applied Mathematics, Vol. 11, pp. 431-441.

[17] Matt, C. F. and Castello, D. A., 2005, ”Modelling and Parameter Estimation of Transmission Lines”, In: Proceedings of the 18th International Congress of Mechanical Engineering, 6-11 November, Ouro Preto, Brazil, Paper 1832.

[18] Meynen, S., Verma, H., Hagedorn, P. and Shäfer, M., 2005, ”On the Numerical Simulation of Vortex-Induced Vibrations of Oscillating Cylinders”, Journal of Fluids and Structures, Vol. 21, pp. 41-48.

[19] Özişik, M. N., 1993, ”Heat conduction”, John Wiley & Sons, Inc., New York, 692p.

[20] Özişik, M. N. and Orlande, H. R. B. 2000, ”Inverse Heat Transfer: Fundamentals and Applications”, Taylor & Francis, 160p.

[21] Papailiou, K. O., 1997, ”On the bending stiffness of transmission line conductors”, IEEE Transactions on Power Delivery, Vol. 12, No. 4, pp. 1576-1588.

[22] Rao, S. S., ”Mechanical Vibrations”, Addison-Wesley Publishing Company, Reading, Massachusetts, 3a edição, 1995, 912p.

[23] Rawlins, C. B., 1979, ”Transmission Line Reference Book: Wind-Induced Conductor Motion”, Ed. EPRI, Palo Alto, California, 244p.

[24] Reddy, J. N., 1993, ”Introduction to the finite element method”, McGraw-Hill, 896p.

[25] Vecchiarelli, J., Currie, I. G. and Havard, D. G., 2000, ”Computational Analysis of Aeolian Conductor Vibration with a Stockbridge-Type Damper”, Journal of Fluids and Structures, Vol. 14, pp. 489-509.

[26] Wagner, H., Ramamurti, V., Sastry, R. V. R. and Hartmann, K., 1973, ”Dynamics of Stockbridge Dampers”, Journal of Sound and Vibration, Vol. 30, No. 2, pp. 207-220.

RESPONSIBILITY NOTICE

The authors are the only responsible for the printed material included in this paper.